

# Damping effects in $^{100}\text{Sn} + ^{16}\text{O}$ and $^{100}\text{Sn} + ^{16}\text{Ca}$ collisions

Hossein Sadeghi\*, Mahdiah Ghafouri

## Abstract

Skyrme Forces (SF) Based Mean Field Model (MFM) or related density function is widely used to describe nuclear states, collective vibrational excitation, and heavy-ion collisions. To investigate  $^{100}\text{Sn} + ^{16}\text{O}$  and  $^{100}\text{Sn} + ^{48}\text{Ca}$  collisions on a 3-dimensional(3D) mesh with Skyrme SV-bas forces in  $E_{cm}=100, 150, \text{ and } 200 \text{ MeV}$ , Time-Dependent Hartree-Fock Skyrme(TDHFS) computations were done. The effective interaction in the computation of reaction dynamics as an important role in understanding the dynamics of the reaction provides us with knowledge about the characteristics of heavy-ion reactions' effective interaction. The effect of increasing the ratio of neutrons to protons and the symmetry and asymmetry of the nuclei, as well as the size of the box at different energies, on the structure of the composite core, was investigated. The  $^{100}\text{Sn} + ^{16}\text{O}$  collision time course findings reveal that the continuous dampening effect remains after the fusion process. The damping mechanism has been demonstrated to be connected to breaking the dependency on box size, which is like the twisted average boundary condition that may avoid box size impacts on the 3D coordinate space employed, whereas periodic boundary conditions are seen for  $^{100}\text{Sn} + ^{48}\text{Ca}$ .

## Keywords

The time-dependent skyrme hartree-fock (TDHFS), Heavy-ion collisions, Quadrupole deformation, Damping effects.

Department of Physics, Faculty of Science, University of Arak, Arak 8349-8-38156, Iran.

\*Corresponding author: H-Sadeghi@araku.ac.ir

## 1. Introduction

The Time-Dependent Hartree-Fock (TDHF) theory is a no-perturbation model for low-energy heavy-ion collisions that describes the transfer of multiple nucleons and is particularly useful in investigating nuclear dynamics [1–7]. When there is enough energy for the Coulomb barrier in low-energy heavy-ion collision reactions, the collision system passes through two original phases: full fusion and overlap of the target and projectile, followed by disintegration into two or more fragments. At low energies, the nucleon's mean free path surpasses the size of the composite system. In contrast, at higher energies, the mean free path of the nucleon decreases and started to drop as the energy increases.

When computer memory and performance were so restricted in the 1970s and 1980s, computations had to make limiting assumptions such as axial symmetry and the removal of spin-orbit pairing. TDHF computations in the 3D Cartesian lattice without symmetry constraints and with significantly more accurate numerical approaches have been achievable over time and with increased computer capability [8–10]. Simultaneously, the quality of effective interactions improved considerably [11–15].

TDHF without pairing is an acceptable approximation for nuclear collisions with higher excited energy. TDHF computations are typically carried out in three-dimensional (3D)

Cartesian space with periodic boundary conditions [16]. For more specific examples of physics applied to the SV-bas interaction, see [17]. The TDHF model is an MFM for the dynamics of particles in nuclear collisions. The microscopic TDHF technique has the advantage of including shell effects, low-energy interactions, and often molecular dynamics models in which Nucleon-Nucleon(NN) collisions may be easily combined. Because of the neutron-proton ratio, data for  $^{100}\text{Sn}$  are few. Furthermore, the energy of individual particles in comparison to  $^{100}\text{Sn}$  is unknown. The data is restricted to the energy distribution between two low-energy orbitals [18, 19], but for higher-energy orbitals, an extrapolation from neighboring nuclei with typical uncertainties of a few hundred keV is provided [20]. The  $^{100}\text{Sn}$  has an almost inert core that may be quickly activated by the addition of particles or holes. As a result, it's an excellent ground-state test for fundamental nuclear models. Another reason for the growing interest in nuclear structure in this field is the nuclear synthesis process [21]. It was recently determined that this reaction chain terminates at around  $^{100}\text{Sn}$ . Furthermore,  $^{100}\text{Sn}$  is anticipated to have a heavier double magic nucleus. In transfer processes and the energy of single particles (holes), the shell closure at  $^{48}\text{Ca}$  has been studied in detail [22].

We recently used the Skyrme-Hartree-Fock-Bogolyubov (SHFB) approach with density-dependent pairing interaction to investigate data such as total binding energy, charge radius,

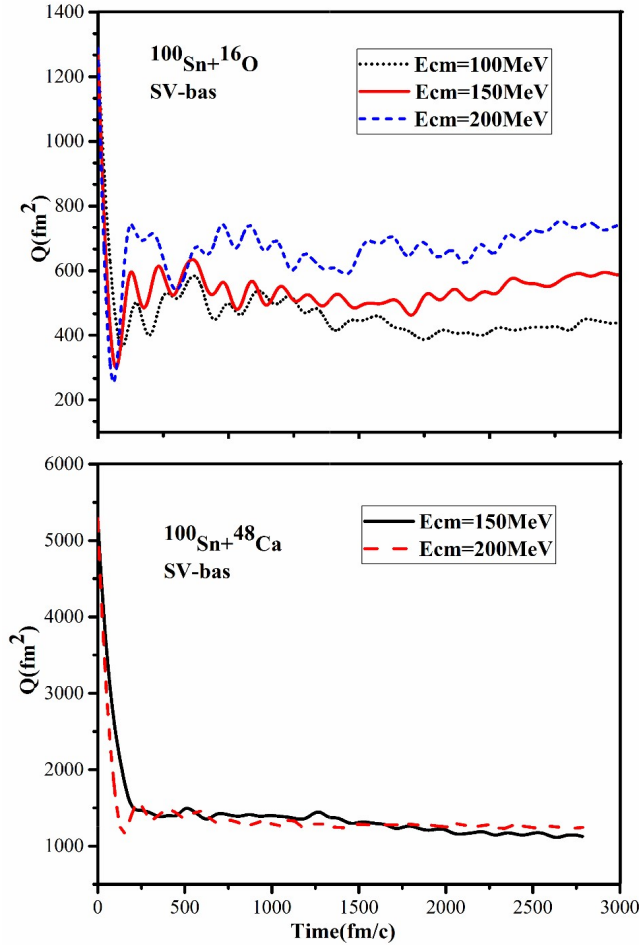


**Figure 1.** The quadrupole momentum for collisions  $^{100}\text{Sn}+^{16}\text{O}$  and  $^{100}\text{Sn}+^{40}\text{Ca}$  of varying energies.

and so on. The null range is calculated using interactions as a function of density throughout the pairing channels [23]. All stable cores exhibit consistent statistical behavior, according to the data. Furthermore, when the mass of the selected nuclei rises, the behavior becomes more uniform. The ratio rise in neutron number in heavy nuclei, on the other hand, suggests higher uniformity in the structure of these nuclei than in lighter nuclei. The average rate of quadrupole deformation in heavy nuclei, on the other hand, is larger than in other mass ranges, and there is a direct relationship between the deformation rate and regular behavior. This may be explained by a combination of rotational and vibrational modes of motion, increasing the regularity of these nuclei's structure.

The following is how this article is organized: Section 2 briefly presents the fundamental principles and theoretical framework, as well as how we derive the numerous observables described in the paper. Section 3 presents our results for the center of mass energies. After the fusion phase, the characteristics of a single particle, the evolution of quadrupole deformation and kinetic energy, rotational amplitude, and the continuum damping effect remain. Section 4 contains a

summary of our results and conclusions.

## 2. Theoretical farmwork

### 2.1 The time-dependent mean-field equations

The TDHF framework is a quantum mechanical framework that employs one-particle wave functions. The initial collision condition at TDHF is derived from the Hartree-Fock (HF) static equations. To derive the wave functions that represent the temporal development of a collision system and the density of space protons and neutrons at any time and location, a set of time-dependent Schrödinger equations is thoroughly solved. Certain limitations in static computations can be employed to solve numerous scenarios beneficial in solving static Hartree-Fock equations. The steady-state equations are generated by using the mean-field equations of single-particle wavefunctions  $\psi_\alpha$  as a starting point:

$$\hat{H}\psi_\alpha = \varepsilon_\alpha\psi_\alpha \quad (1)$$

$\hat{H}$  is the Hamiltonian in the mean-field. The single-particle energy for "the place" is shown by  $\varepsilon_\alpha$ . Since different scattering investigations have revealed that nucleons move with kinetic energy (10 MeV) inside nuclei, this energy is compared to nucleon inertial energy, which is approximately (1000 MeV). Regardless of the relativistic effects of nucleon mobility, we may examine the energy spectrum of nuclei using non-relativistic quantum mechanics using the Schrödinger equation, which is a non-relativistic equation. The ground state of a nucleus with single-particle wave functions  $\psi_\alpha(\mathbf{r})\exp(-i\varepsilon_\alpha t/\hbar)$  is expressed as follows [24]

$$\left[\frac{-\hbar^2}{2m}\nabla^2 + V(\rho(\psi))\right]\psi_\alpha(\mathbf{r}) = \varepsilon_\alpha\psi_\alpha(\mathbf{r}) \quad (2)$$

This results in a static solution with the phase factor:

$$e^{i\mathbf{k}\cdot\mathbf{r}}\psi_\alpha\left[\mathbf{r} - \frac{\hbar\mathbf{k}}{m}t\right] \quad (3)$$

When the Hamiltonian single particle is Galileo-invariant, this time-dependent equation is solved. To obtain the net density dependence, we must supplement the density function with expressions comprising rotating currents and currents. Certain limitations in static computations can be employed to solve numerous scenarios beneficial in solving static Hartree-Fock equations. The most commonly used constraint is the expectation value constraint used in the quadrupole  $\langle\psi_\alpha|H - \lambda Q_{20}|\psi_\alpha\rangle$ . We may show this by including a limit containing a possible theorem in the single-particle Hamiltonian, as in the case of quadrupoles

$$\hat{H} \rightarrow \hat{H} - \lambda(2z^2 - x^2 - y^2) \quad (4)$$

Because the employed numerical approach does not limit the deformation, take note outside for unstable constraints like quadrupoles, which might reach significant values near the computation box's boundaries and pull the wave function

there. Depending on how the system modes and desired observations are adjusted, the TDHF equations can be evaluated in Slater determinant wavefunction space [5] or derived using TDHF. The sources [25, 26] analyze the TDHF equations based on the Schrödinger equation as a function of time.

$$i\hbar \frac{\partial}{\partial t} |\psi_\alpha(t)\rangle = \hat{H} |\psi_\alpha(t)\rangle \quad (5)$$

The static wave functions are displayed as  $\psi_{\alpha,I}^{static}(t)$  that  $I = 1; 2$  labels the two nuclei.  $\psi_{\alpha,I}^{static}(\mathbf{r}-\mathbf{R},\mathbf{s})$  is achieved using grid interpolation. The numerical box for collisions must be bigger than the numerical box for static Hartree-Fock computations. The Slater state is the initiating configuration for nuclear reactions, with shifted and increased single-particle wavefunctions, as seen in Ref. [16]. A Hamiltonian in interaction may also be defined as follows

$$\hat{H} = \hat{T} + \hat{V} = \sum_{\alpha\beta} t_{\alpha\beta} a_\alpha^\dagger a_\beta + \frac{1}{2} \sum_{\alpha\beta\gamma\delta} V_{\alpha\beta\gamma\delta} a_\alpha^\dagger a_\beta^\dagger a_\delta a_\gamma \quad (6)$$

$t_{\alpha\beta}$  is the kinetic energy and  $V_{\alpha\beta\gamma\delta}$  is the two-body interaction matrix elements. Also  $a_i^\dagger$  and  $a$  create and annihilate a particle in the state  $i$ , respectively.

The TDHF equations are obtained as follows

$$S = \int dt [E(\psi_\alpha) - \sum_\alpha \langle \psi_\alpha | i\partial_t | \psi_\alpha \rangle] \quad (7)$$

The code's mean-field equations are based on the skyrme energy functional, as shown in Ref. [16]. The following integral equation can be used to solve TDHF

$$|\psi_\alpha(t + \Delta t)\rangle = U(t, t + \Delta t) |\psi_\alpha(t)\rangle$$

$$U(t + \Delta t) = \hat{T} e^{(-\frac{i}{\hbar} \int_t^{t+\Delta t} \hat{H}(t) dt)} \quad (8)$$

$\hat{U}$  and  $\hat{T}$  are the time-evolution and the time-ordering operations, respectively.

The TDHF dynamics reported in this paper are derived from the Sky3D algorithm, which was designed to solve the Hartree-Fock static and time-dependent equations in a broad 3D geometry. The reference [16] has a full discussion of the code's physics and administration. This model is based on the global shape's functional skyrme energy [16]. The code's mean-field equations are based on the skyrme energy function. Current reviews may be found in [12, 13]. Without taking into account pairing, the energy is depicted as

$$E = E_{kin} + \int d^3r (\varepsilon_{Sk} + \varepsilon_{Sk}^{IS}) + E_c \quad (9)$$

where energy is

$$E_{kin} = \int d^3r \frac{\hbar^2}{2m} \tau \quad (10)$$

and the following equations there are several terms derived from the skyrme force

$$\varepsilon_{Sk} = \frac{1}{2} b_0 \rho^2 + b_1 (\rho \tau - \mathbf{J}^2) - \frac{b_2}{2} \rho \Delta \rho + \frac{b_3}{3} \rho^{\alpha+2}$$

$$- \sum (\frac{b_0}{2} \rho_q^2 + b_1 (\rho_q \tau_q - \mathbf{J}^2) + \frac{b_2}{2} \rho_q \Delta \rho_q + \frac{b_3}{2} \rho^\alpha \rho_q^2) \quad (11)$$

The code solves mean-field equations using the skyrme energy function, which is frequently used. As a starting point, we examine distorted harmonic oscillator wave functions (*nof* = 0). This is just for static computations. Harmonic oscillator states with primary radius in three dimensions yield primary wave functions. Asymmetric nuclei are given three separate radiuses to prevent being inserted in a symmetrical composite. The *nmeut* and *nprot* code inputs, which indicate the number of neutrons and protons, define the core type, while *npsi* can be used to add some empty modes (this sometimes leads to faster convergence). The number of nodes in each direction distinguishes them. The following terms are also added after considering the contribution of the spin current terms

$$\varepsilon_{Sk}^{IS} = -b_4 [\rho \nabla \cdot \mathbf{J} + \sigma \cdot (\nabla \times \mathbf{J})] + b_4 \sum_q [\rho_q \nabla \cdot \mathbf{J}_q + \sigma_q \cdot (\nabla \times \mathbf{J}_q)] \quad (12)$$

The Coulomb energy is as follows

$$E_c = \frac{e^2}{2} \int d^3r d^3r' \rho_p(\mathbf{r}) \frac{1}{|\mathbf{r} - \mathbf{r}'|} \rho_p(\mathbf{r}') - \frac{3}{4} e^2 \left(\frac{3}{\pi}\right)^{\frac{1}{3}} \int d^3r [\rho_p(\mathbf{r})]^{\frac{4}{3}} \quad (13)$$

with

$$\sigma_q(\mathbf{r}) = \sum_q \varphi_\alpha^+(\mathbf{r}) \hat{\sigma} \varphi_\alpha(\mathbf{r})$$

$$\mathbf{J}_q(\mathbf{r}) = -i \sum_q \varphi_\alpha^+(\mathbf{r}) \nabla \times \hat{\sigma} \varphi_\alpha(\mathbf{r})$$

That  $q = p$  for protons and  $q = n$  for neutrons and  $\rho = \rho_p + \rho_n$  is total density.  $b_3$  is defined by the  $t$  and  $x$  coefficients contained in the skyrme force description, as shown in Ref. [16]. The Sabroton *hpsi* mean-field module must be used to determine additional contributions to single-particle hamiltonin. The code must be applied, and the result must be added to the output wave function's output to calculate how additional expressions act on the input wave function. Again, spatial derivatives might be applied in different loops for efficiency. To compute total energy, we employ a 3D solver (TDHFS) that solves the self-consistent HF equation as well as the TDHF equation. For further information, see [16].

## 2.2 Boundary conditions

The periodic boundary condition is a logical choice for expressing plane waves and is useful in 3D unitary network calculations. TBC [16], also known as a generalized block boundary condition, is expressed as [27]

$$\psi(r + nL) = e^{i\theta \cdot n} \psi(r) \quad (14)$$

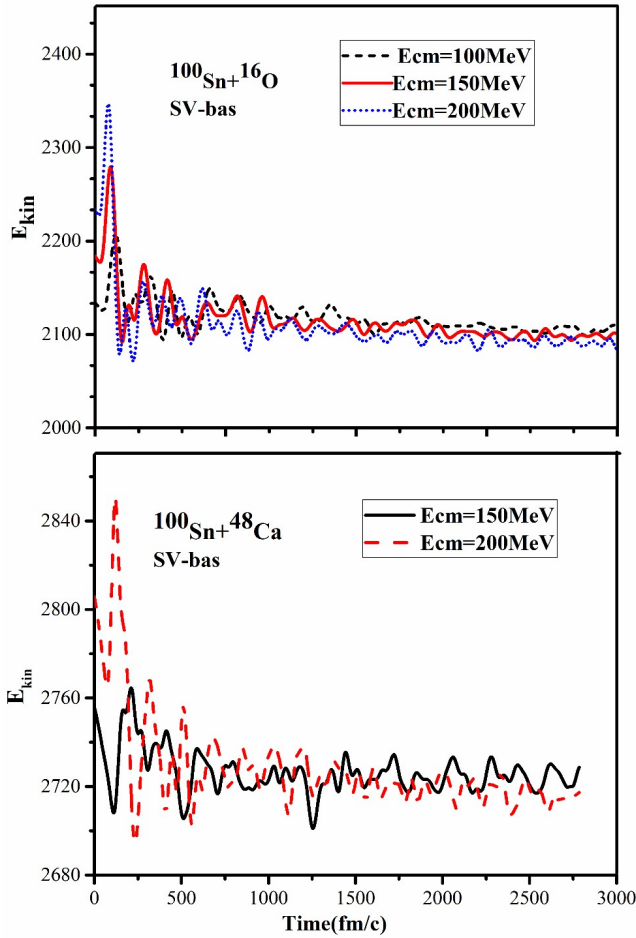


**Figure 2.** Kinetic energy results for collisions  $^{100}\text{Sn}+^{16}\text{O}$  and  $^{100}\text{Sn}+^{40}\text{Ca}$  of varying energies.

In 3D Cartesian coordinates,  $r$  denotes the 3D coordinates,  $L$  the box size, and  $n$  the unit vector. The twist angle ranges from 0 to  $180^\circ$  degrees. We get the periodic boundary condition if the twist angle is equal to zero.

The HP equation of a single particle can be written as:

$$\hat{H}_\theta \psi_{\alpha\theta}(r) = \varepsilon_{\alpha\theta} \psi_{\alpha\theta}(r) \quad (15)$$

The discrete state of the one-particle wave function is shown by  $\psi$ . For further information, see [28].

### 2.3 Multipole moment

In the mean-field Hamiltonian, we employ the skyrme SV-bas interaction for nucleons in the TDHF computations. Numerical computations are carried out using a three-dimensional Cartesian grid. Many experimental experiments have been conducted to investigate the low-energy features of even-even isotopes of existing nuclei, including Sn. Multipole moments characterize the majority of density distribution features. The center of mass is the most significant of them (c.m). Spherical moments in the quadrupole state are defined as follows:

$$Q_{2m}^{(type)} = \int d^3r r^2 Y_{2m} \rho^{(type)}(\mathbf{r} - \mathbf{R}) \quad (16)$$

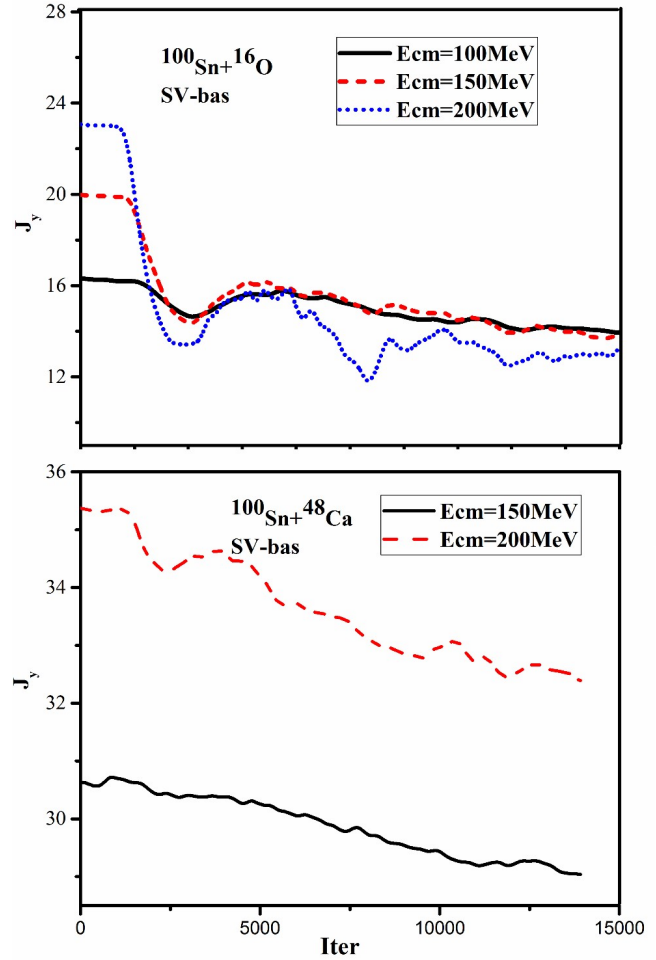


**Figure 3.** Results of angular momentum temporal evolution for  $^{100}\text{Sn}+^{16}\text{O}$  and  $^{100}\text{Sn}+^{40}\text{Ca}$  of varying energies.

The Cartesian quadrupole in this code reads

$$Q = 2 \sin\left(\frac{\pi z}{z_{box}}\right)^2 - \sin\left(\frac{\pi y}{y_{box}}\right)^2 - \sin\left(\frac{\pi x}{x_{box}}\right)^2 \quad (17)$$

There are two shape parameters  $a_0$  and  $a_2$  called deformation  $\beta$  and triaxiality  $\gamma$  called Bohr-Mottelson parameters.

$$\beta = \sqrt{a_0 + 2a_2}, \gamma = a \tan\left[\frac{\sqrt{2}a_2}{a_0}\right] \quad (18)$$

Single-particle energies allow more detailed energy data. Because the monopolar momentum is proportional to the total number of particles, the radius *r.m.s.* is commonly employed to characterize monopolar oscillations. Alternatively, their square is utilized as

$$r_{rms}^{type} = \sqrt{\frac{\int d^3r r(\mathbf{r} - \mathbf{R})^2 \rho^{type}(\mathbf{r})}{\int d^3r \rho^{type}(\mathbf{r})}} \quad (19)$$

The “type” can be a proton, a neutron, or total density.

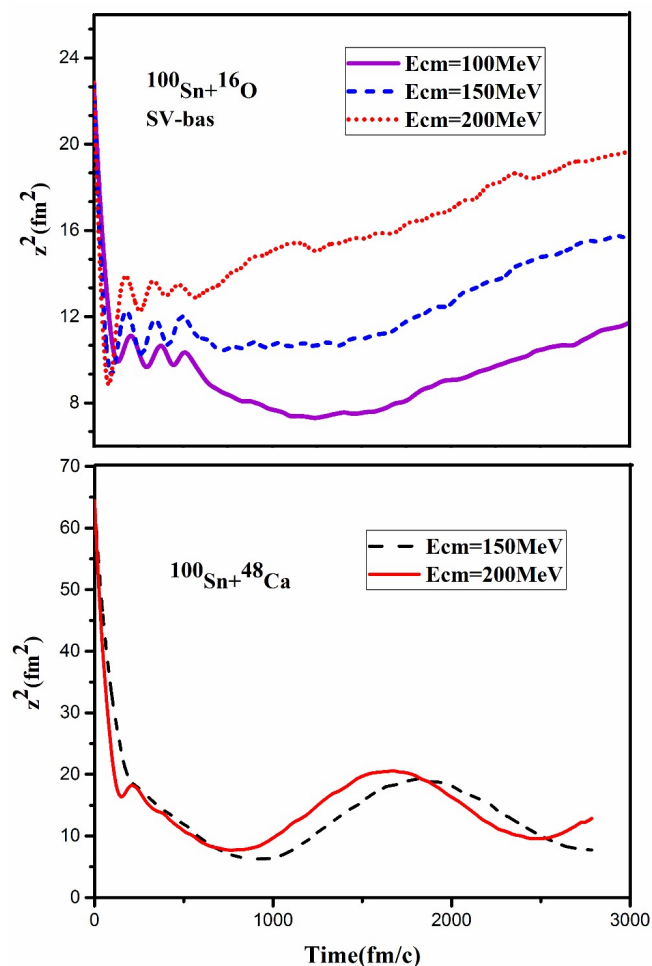


**Figure 4.** Results of  $z^2$  temporal evolution for collisions  $^{100}\text{Sn}+^{16}\text{O}$  and  $^{100}\text{Sn}+^{40}\text{Ca}$  of varying energies with collision parameter  $2fm$ .

### 3. Results and discussion

Nuclear collision is a key application of nuclear TDHF. Unlike high-energy collisions, when reaching equilibrium before the end of the response time is impossible, low-energy collisions can have several sorts of equilibria, each on a distinct time scale. During the first phase, a fast charge balance is formed as a result of nucleon migration near the Fermi surface. The mechanism of this equilibrium may be interpreted as the extension of a single particle's motion from one nucleus to the other once the potential barrier between two colliding nuclei is reduced following contact. This procedure may be completed in a fraction of a second. Charge balancing is critical because it prevents unusual particles with substantial proton-neutron asymmetry from forming. Nuclear fission can be trapped in opposing components of a system when it collides, resulting in a higher proton-neutron imbalance than the system before fission. When the Coulomb effects are included, the proton-neutron imbalance grows to the greatest density measured. With increased beam energy, the influence of the initial state

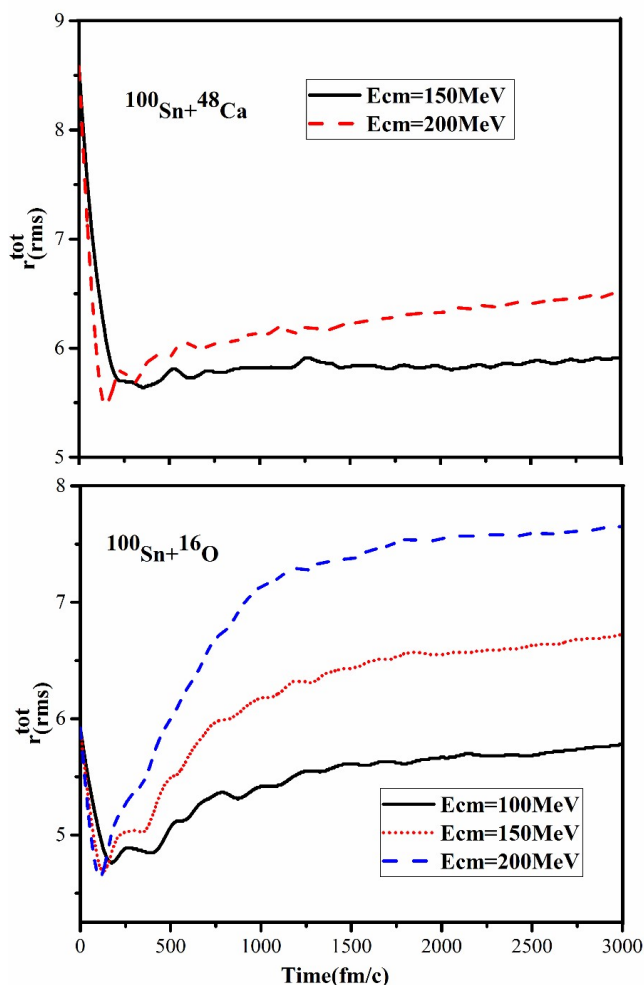


**Figure 5.** Comparison of  $r_{rms}^{tot}$  obtained for  $^{100}\text{Sn}+^{16}\text{O}$  and  $^{100}\text{Sn}+^{40}\text{Ca}$  of varying energies.

shell is reduced. The motion equilibrium, which depicts the balance between nuclear forces and coulomb, is projected to last 10 to 20 seconds. In low-energy collisions, slower equilibrium processes such as thermal equilibrium and some composite system fission or decay processes can also persist longer than 10–15 seconds. This code is intended to make such collision circumstances more obvious.

We do TDHF 3D collision simulations with Sky3D code and two magic shells with two projectiles, but in one we detect symmetry in the number of protons and neutrons, while in the other we don't see the asymmetry in the various energies of neutrons and protons. We know that the initial shell effect rises as the energy in the beam increases. Quadrupole momentum is atomic nuclei feature that is used in a range of research, measurement, and nuclear investigations.

The temporal changes of the quadrupole deformities arising from the TDHF computations of the aforesaid collisions are shown in Fig. 1. The oscillations are severely damped at large amplitudes during the fusion phase. At larger impact energy, the gradients are stronger. The deformation, on the other hand,

is always near to each other. The variations in kinetic energy deformation are not symmetrical. Melting, since it is density-dependent and incompressible, is more than just a damping oscillator for quadrupole deformations.

The time evolution of the total kinetic energy for  $^{100}\text{Sn}+^{16}\text{O}$  and  $^{100}\text{Sn}+^{40}\text{Ca}$  with impact energies is shown in Fig. 2. The kinetic energies' distortion vibrations are not symmetrical. Because bigger quadrupoles at higher impact energy are not always associated with larger axial ratios, we may conclude that the volume expansion of the composite nucleus is at work in this scenario. Fig. 2 depicts the respective final kinetic energies. These disparities suggest that kinetic energy has been converted into potential energies. The final kinetic energies are lesser and the quadrupole deformation energies are bigger with higher impact energy. By investigating the collision with the  $2\text{ fm}$  collision parameter, we discovered the boundary condition in the Skyrme Hartree-Fock time-dependent collision calculation done in 3D coordinate spaces and discovered that the rotation amplitude is likewise damped.

The time evolution of the angular momentum  $J_y$  for  $^{100}\text{Sn}+^{16}\text{O}$  and  $^{100}\text{Sn}+^{40}\text{Ca}$  collisions is depicted in Fig.3. Even though the density distribution is spherical, the angular momentum  $J_y$  is not steady. Furthermore, total angular momentum is not conserved. The cushioning range is larger independent of the maximum impact energy, as seen in the figure. To deal with periodic boundary conditions for  $^{100}\text{Sn}+^{16}\text{O}$ , the oscillation is seen to be slightly cosine-shaped in the lower stages, but as the stages advance, we detect a substantial damping effect, which is connected to breaking the reliance on box size. When we investigated the collision with the  $2\text{ fm}$  impact parameter, we discovered that the range of rotation diminishes as well. If no damping is seen for the  $^{100}\text{Sn}+^{40}\text{Ca}$  collision and there is no dependence on the size of the box, the rotation is nearly a full cosine function up to this computation step. The amplitude of rotation is damped in the calculations, as seen in the figure; this rotational damping is not surprising given the acceptable damping of small-amplitude vibrations.

The values of  $z^2$  for different collision energies, as well as the  $^{100}\text{Sn}$  collision with  $^{16}\text{O}$  and  $^{40}\text{Ca}$  with varying energies, are provided in Fig. 4. The Coulomb repulsive strength between protons is stated to be overcome in stable nuclei due to the presence of additional neutrons (N/Z) in their scheme. The findings also reveal a consistent statistical tendency for all stable nuclei studied. Furthermore, the more consistent behavior grows as the mass of the selected nuclei increases. Our objective is to investigate the characteristics of stable nuclei in collisions of various mass ranges, as well as the effect of various factors such as rotation, quadrupole deformation rate, and so on. In the results, increasing the mass of the selected nuclei and taking into account the symmetry and asymmetry of the nuclei, as well as the box size, resulting in a regular statistical behavior for the stable nuclei investigated.

A remarkable hybrid system is constructed for  $E_{cm} = 150$  and  $200\text{ MeV}$  in collision and  $E_{cm} = 100, 15,$  and  $200\text{ MeV}$  in collision. The overall radius in Fig. 5 depicts how the

system compresses and changes over time. Its value grows again when it approaches fusion or when the cores split. This helps you to determine if they are sufficiently far to prevent unexpected occurrences from occurring. The rationale for extending the box is that operators, unlike orbital angular momentum, are not periodic since the vector itself is not periodic but leaps over the limit. The nuclei deviate and then depart the calculation box at the lower center of mass energies, as shown in the calculations. To avoid this, end the computation when the distance between the cores exceeds the distance between the centers of mass of the two independent nuclei, which should generally be set somewhat more than the original distance. This demonstrates that the answer has a distorted average boundary condition and is of the generalized periodic boundary condition type.

According to the figures, the reaction is comparable to the twisted mean boundary condition in gigantic resonance TDHF calculations, which is a generalized periodic boundary condition for block waves with non-zero twist angles. The twisted mean boundary condition findings with intermediate twist angles can considerably balance out the effects of limited box size in density material physics [29]. The reaction  $^{100}\text{Sn}+^{40}\text{Ca}$ , on the other hand, includes general boundary conditions [28].

#### 4. conclusion

In this paper, we look at the Sky3D code, which operates in 3D coordinate spaces. The damping mechanism, as we can see, refers to the removal of the dependency on the size of the box in the twisted limit state. We discovered that the rotational amplitude is attenuated in a collision with the  $2\text{ fm}$  impact parameter in the  $^{100}\text{Sn}+^{16}\text{O}$  collision. Using Skyrme powers results in new impacts and unexpected complications. Because of the existence of additional neutrons (N/Z), stable nuclei may overcome the Coulomb repulsive force between protons. Furthermore, the structure of these nuclei as a result of the increase in binding energy is determined by the resulting arrangement of different layers that are complete and eventually have almost spherical shapes, providing an excellent opportunity to study the effect of rotation and deformation on the structure of the nuclei. The proportional increase in the number of neutrons in heavy nuclei, on the other hand, indicates a stronger order in the structure of these nuclei than in lighter nuclei. Heavy nuclei have a greater average quadrupole strain rate than other mass ranges, and there is a real correlation between elastic modulus and regular behavior. This increase in order can be justified by a combination of rotational and vibrational states, increasing in the order of these nuclei's structure. The influence of the distance between nuclei relative to their centers of mass at various energies on the demand for nuclear fusion was investigated. It's intriguing to see how these effects hold up in heavier systems that are more symmetrical and asymmetrical. Further applications of twisted boundary conditions in nuclear processes involving weakly bound nuclei will be valuable.

**Conflict of interest statement:**

The authors declare that they have no conflict of interest.

## References

- [1] J. W. Negele. *Reviews of Modern Physics*, **54**:9135, 1982.
- [2] T. Nakatsukasa, K. Matsuyanagi, M. Matsuo, and K. Yabana. *Reviews of Modern Physics*, **88**:045004, 2016.
- [3] C. Simenel. *European Physical Journal A*, **48**:152, 2012.
- [4] A. S. Umar and V. E. Oberacker. *Nuclear Physics A*, **944**:238, 2015.
- [5] L. Guo, J. A. Maruhn, P. G. Reinhard, and Y. Hashimoto. *Physical Review C*, **77**:041301R, 2008.
- [6] G. Scamps and D. Lacroix. *Physical Review C*, **87**:014605, 2013.
- [7] P. Goddard, P. Stevenson, and A. Rios. *Physical Review C*, **92**:054610, 2015.
- [8] A. S. Umar and V. E. Oberacker. *Physical Review C*, **73**:054607, 2006.
- [9] K. Washiyama and D. Lacroix. *Physical Review C*, **78**:024610, 2008.
- [10] D. J. Kedziora and C. Simenel. *Physical Review C*, **81**:044613, 2010.
- [11] E. Chabanat, P. Bonche, P. Haensel, J. Meyer, and R. Schaefferb. *Nuclear Physics A*, **635**:231, 1998.
- [12] M. Bender, P. H. Heenen, and P. G. Reinhard. *Reviews of Modern Physics*, **75**:121, 2003.
- [13] P. Klüpfel, P.G. Reinhard, T. J. Bürvenich, and J. A. Maruhn. *Physical Review C*, **79**:034310, 2009.
- [14] S. Goriely, S. Hilaire, A. J. Koning, M. Sin, and R. Capote. *Physical Review C*, **79**:024612, 2009.
- [15] M. Kortelainen, T. Lesinski, J. Moré, W. Nazarewicz, J. Sarich, N. Schunck, M. V. Stoitsov, and S. Wild. *Physical Review C*, **82**:24313, 2010.
- [16] J. A. Maruhn, P. G. Reinhard, P. D. Stevenson, and A. S. Umar. *Computer Physics Communications*, **185**:2195, 2014.
- [17] Y. Iwata. *Modern Physics Letters A*, **30**:155008, 2015.
- [18] D. Seweryniak, M. P. Carpenter, S. Gros, A. A. Hecht, N. Hoteling, R. V. F. Janssens, T. L. Khoo, T. Lauritsen, C. J. Lister, G. Lotay, D. Peterson, A. P. Robinson, W. B. Walters, X. Wang, P. J. Woods, and S. Zhu. *Physical Review Letters*, **99**:022504, 2007.
- [19] I. G. Darby, R. K. Grzywacz, J. C. Batchelder, C. R. Bingham, L. Cartegni, C. J. Gross, M. Hjorth-Jensen, D. T. Joss, S. N. Liddick, W. Nazarewicz, S. Padgett, R. D. Page, T. Papenbrock, M. M. Rajabali, J. Rotureau, and K. P. Rykaczewski. *Physical Review Letters*, **105**:162502, 2010.
- [20] H. Grawe, K. Langanke, and G. Martinez-Pinedo. *Reports on Progress in Physics*, **70**:1525, 2007.
- [21] H. Schatz, A. Aprahamian, V. Barnard, L. Bildsten, A. Cumming, M. Ouellette, T. Rauscher, F. K. Thielemann, and M. Wiescher. *Physical Review Letters*, **86**:3471, 2001.
- [22] H. Grawe and M. Lewitowicz. *Nuclear Physics A*, **693**:116, 2001.
- [23] M. Ghafouri, H. Sadeghi, and M. Torkiha. *Results in Physics*, **8**:734, 2018.
- [24] Y. M. Engel, D. M. Brink, K. Goeke, S. J. Krieger, and D. Vautherin. *Nuclear Physics A*, **249**:215, 1975.
- [25] D. J. Rowe, L. E. H. Trainor, and S. S. M. Wong. *Dynamic Structure of Nuclear States*. University of Toronto Press, 1th edition, 1972.
- [26] S. E. Koonin. *Hydrodynamic Approximations to Time-Dependent Hartree-Fock*. dspace.mit.edu, 1th edition, 1975.
- [27] B. Schuetrumpf, W. Nazarewicz, and P. G. Reinhard. *Physical Review C*, **93**:054304, 2016.
- [28] C. Q. He, J. C. Pei, Y. Qiang, and N. Fei. *Physical Review C*, **99**:054318, 2019.
- [29] C. Lin, F. H. Zong, and D. M. Ceperley. *Physical Review E*, **64**:016702, 2001.